Supporting information for

Expanding Interlayer Spacing in MoS_2 for Realizing an Advanced Supercapacitor

Debasish Sarkar*[⊥] [†§], Debanjan Das [⊥‡], Shyamashis Das [†], Ankit Kumar [†], Satish Patil[†], Karuna Kar Nanda [‡], D. D. Sarma[†] and Ashok Shukla*[†]

[†]*Solid State and Structural Chemistry Unit, Indian Institute of Science, Bengaluru-560012, India.*

[‡]*Materials Research Centre, Indian Institute of Science, Bengaluru-560012, India.*

[§]*Department of Physics, Malaviya National Institute of Technology Jaipur, Rajasthan-302017, India.*

*Corresponding Authors: E-mail: akshukla2006@gmail.com (AKS) and

deb.sarkar1985@gmail.com & debasish.phy@mnit.ac.in (DS)

[⊥]Authors contributed equally to this work

Calculation of capacitance, energy and power densities for single electrode and ASC cell

Areal capacitance (*Ca*, mF/cm^2) was calculated from the Cyclic voltammogram data using the equation:

$$C_a = \frac{\int i dt}{a\Delta V} \quad (1)$$

where, i (mA) is the cathodic or anodic current; dt (s) is the time differential, ΔV (V) be the potential window, and a (cm^2) is the effective area of the individual redox active materials for single electrode measurements.

From Galvanostatic charge-discharge data also, areal capacitance (*Ca*, mF/cm^2) values for the electrodes were calculated using equation:

$$C_a = \frac{i\Delta t}{a\Delta V} \quad (2)$$

where, i (mA) is the discharge current, Δt (s) is the discharge time for discharge window ΔV (V) and a (cm^2) is the effective area of the active materials.

Volumetric capacitance (C_V) of electrode materials was calculated by simply replacing area (a) with the volume (V) of electroactive materials in equations (1) and (2), calculated after measuring the thickness of electroactive material on metallic foil using cross-sectional SEM as shown below.

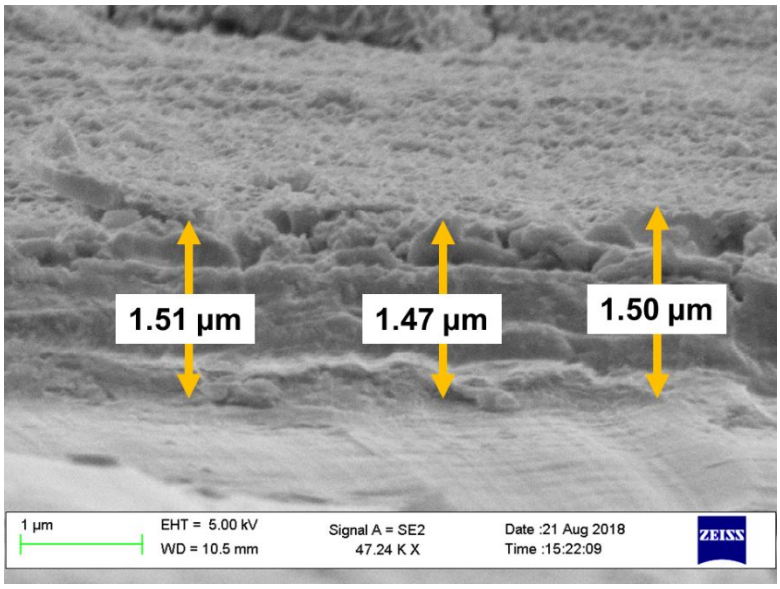

Average thickness of MoS_2/r-GO layer grown on one side of Mo foil is found to be 1.5 µm. Now, considering MoS_2/r-GO layer formed on both sides of the Mo foil during hydrothermal synthesis, total thickness of the electroactive layer would be ~ 3 µm.

However, for the cell, volume (V) represents the total volume (in cm^3) of the device stack including electrodes, separator with electrolyte and PET wrapping and is calculated to about 0.045 cm^3.

Volumetric energy (W, mWh/cm^3) and power densities (P, mW/cm^3) for the fabricated cell were calculated using equations:

$$W = \frac{1}{2} C_V \Delta V^2 \quad (3)$$

$$ESR = \frac{iR\text{-drop}}{2 \times i} \quad (4)$$

and

$$P = \frac{\Delta V^2}{4 \times ESR \times V} \quad (5)$$

where, *i* (mA) is the discharge current; ΔV (V) is the discharge voltage, C_V is the volumetric capacitance, and *ESR* is the equivalent series resistance of the device.

Characterization of as-prepared samples

Detailed morphological and structural characterization of as-prepared samples were carried out using field-emission scanning electron microscope (FESEM), transmission electron microscope (TEM), high-resolution TEM (HRTEM), energy-dispersive X-ray spectroscopy (EDS), and X-ray diffraction (XRD). Color mapping of individual constituent elements present in the samples was performed using electron energy loss spectroscopy (EELS) technique associated with the TEM instrument. Raman measurements were performed on WITec Raman confocal microscope at room temperature using a Nd:YAG laser (532 nm) as an excitation source. X-ray photoelectron spectroscopic (XPS) technique was employed further to investigate the valence states of individual ionic species present in the nanostructured materials.

Electrochemical characterizations for individual electrode materials were carried out on an electrochemical work station (AutoLab PGSTAT 302N) in three-electrode mode, comprising the as-prepared sample as working electrode, a Pt foil as counter electrode and a Saturated Calomel Electrode (SCE, Hg/Hg_2Cl_2) as reference electrode in 1M aqueous Na_2SO_4 solution. The full-cell characterizations were performed on the same work station in two-electrode configuration with reference and counter electrodes shorted. Electrochemical impedance spectroscopy (EIS) studies for individual electrodes and the as-assembled hybrid SC were carried out within the frequency range between 10 mHz and 100 kHz with an operating ac field amplitude of 5 mV.

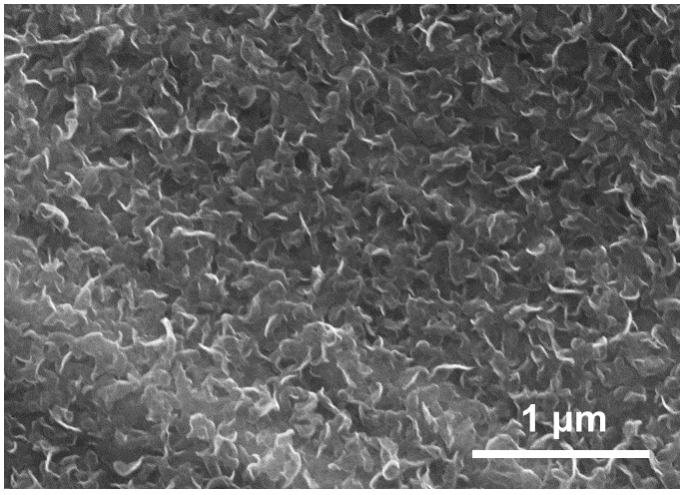

Figure S1 FESEM image of pristine MoS_2 nanoflakes grown on Mo substrate.

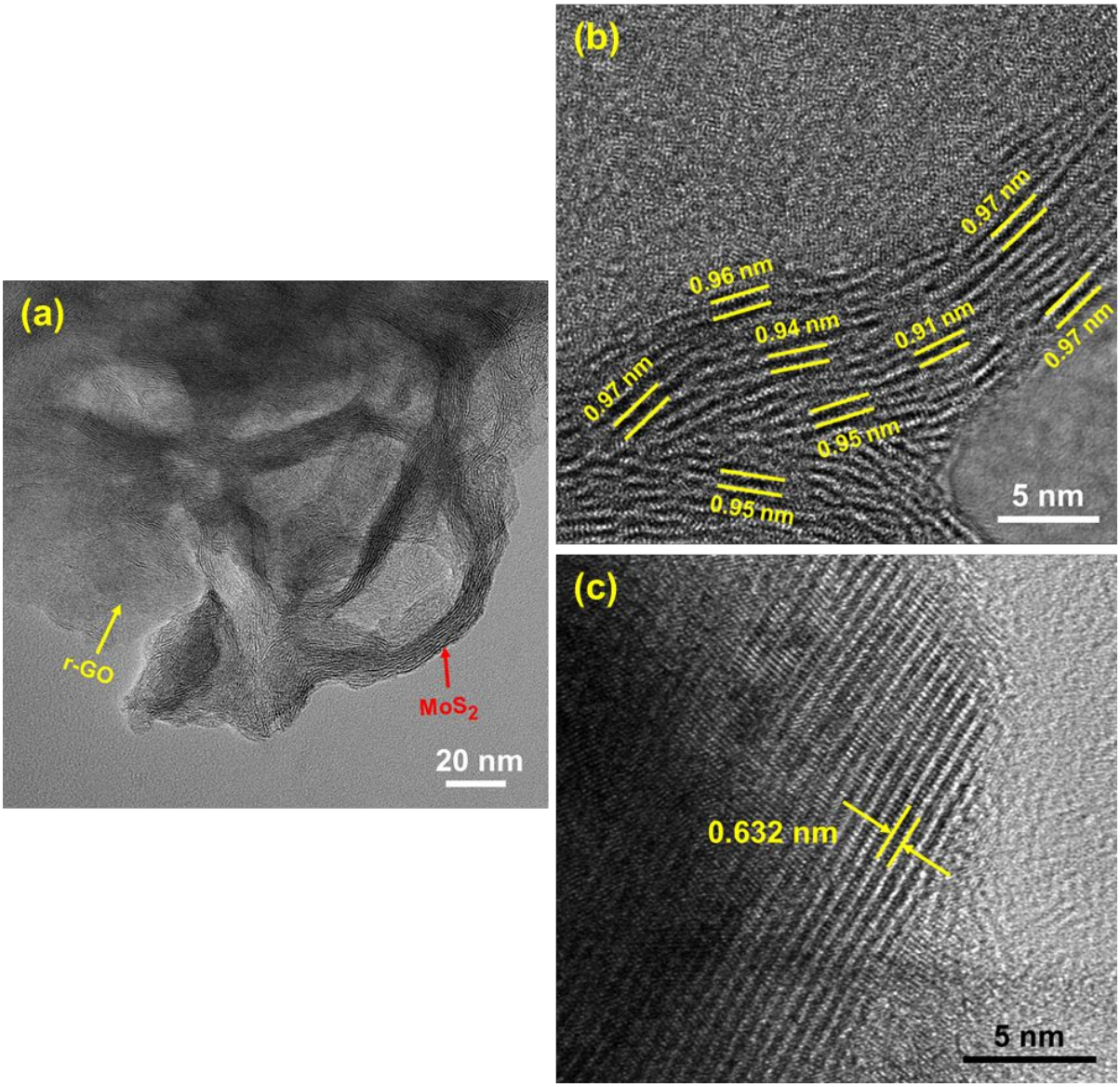

Figure S2 (a) TEM image of MoS_2/r-GO hybrid nanoflakes showing intertwined structure of MoS_2 and r-GO; (b) high-resolution TEM suggests the interlayer spacing of MoS_2 within the range of 0.91 nm to 0.97 nm; and (c) HRTEM image of standard MoS_2 showing the interlayer spacing to be 0.63 nm.

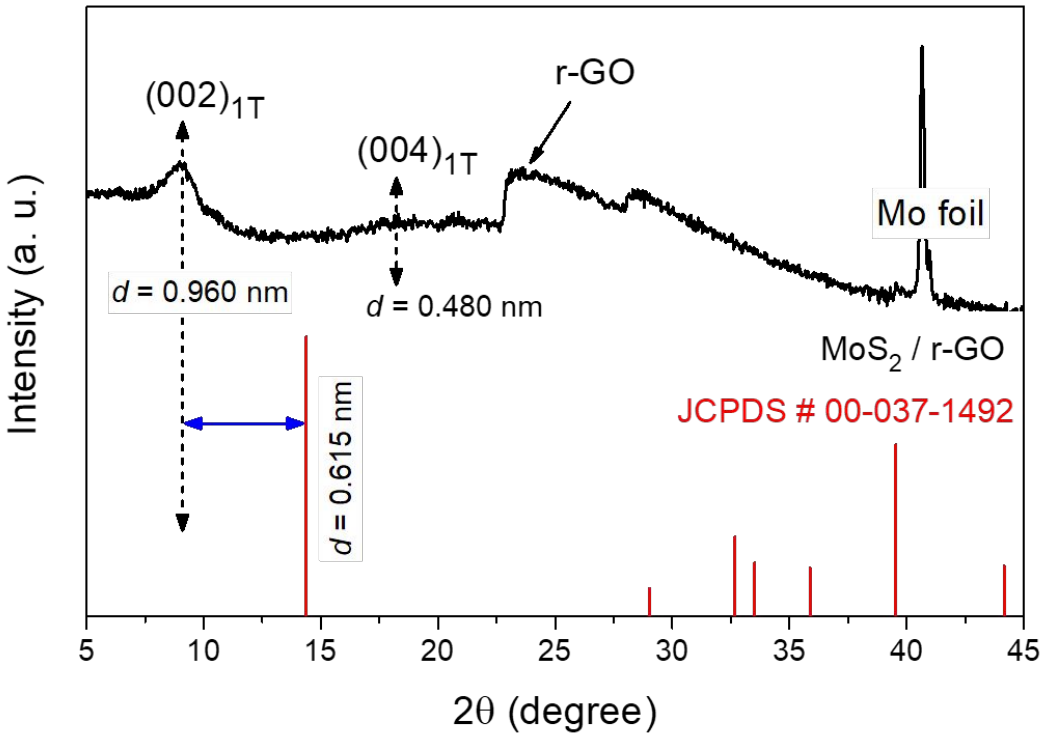

Figure S3 XRD spectrum of MoS_2/r-GO nanoflakes grown on Mo foil along with the XRD pattern of standard MoS_2 (JCPDS card # 00-037-1492).

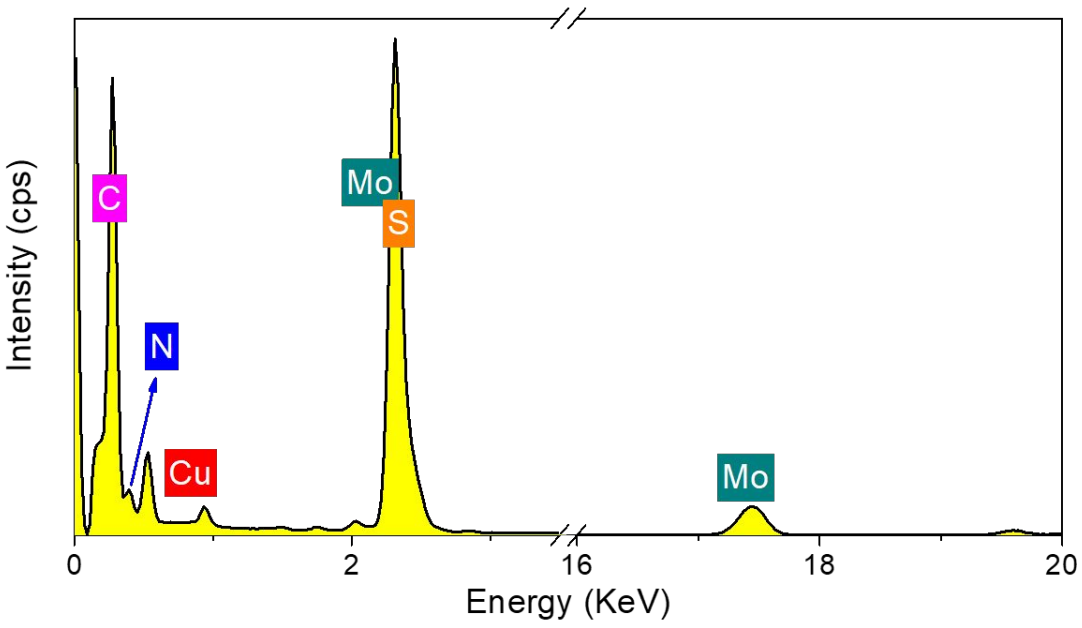

Figure S4 EDS spectrum of MoS_2/r-GO hybrid material shown in Figure 1(d). The spectrum suggests the presence of Mo and S coming from MoS_2 and the N coming from intercalated ammonium ions (NH_4^+) inside MoS_2 interlayers.

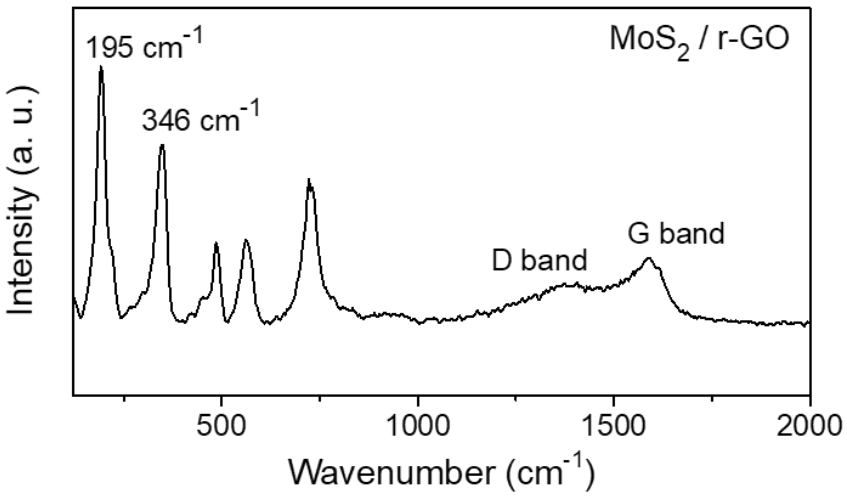

Figure S5 Raman spectra of MoS_2/r-GO hybrid material. Two prominent Raman modes around 1380 cm^{-1} (D band) and 1590 cm^{-1} (G band) correspond to respective D and G bands of r-GO in the hybrid structure.

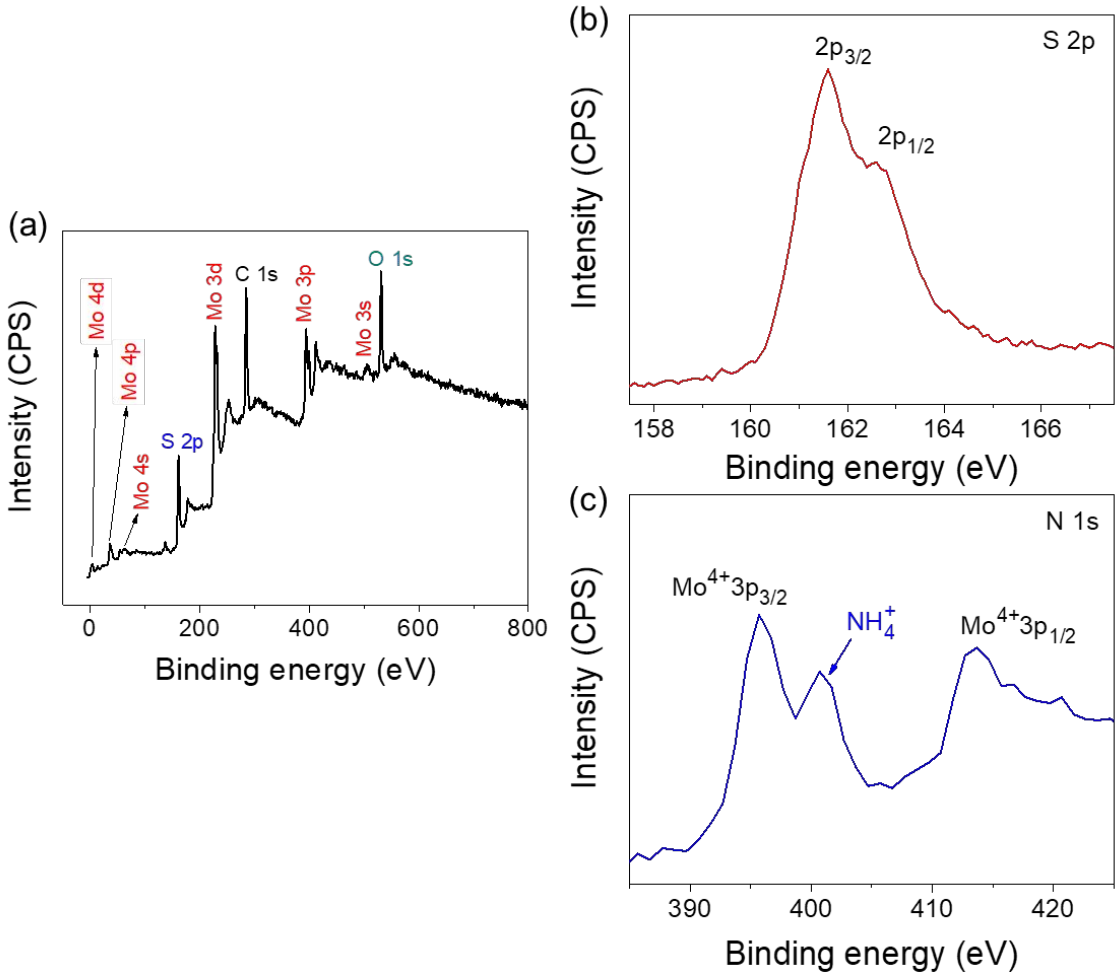

Figure S6 (a) XPS survey spectrum of MoS_2/r-GO hybrid; (b) and (c) show the S 2*p* and N 1*s* regions of the XPS spectrum.

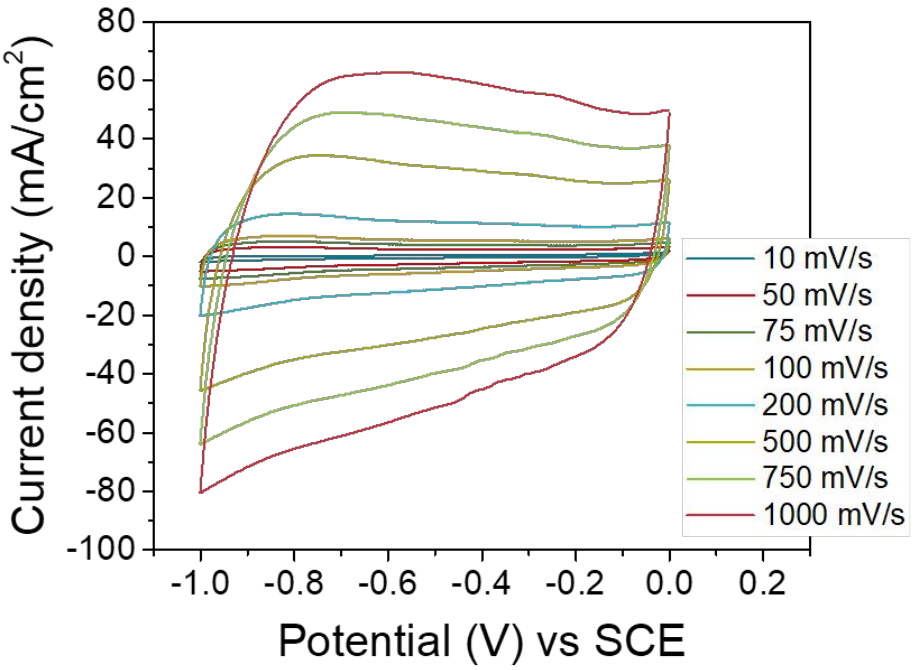

Figure S7 CV profiles for pristine MoS_2 nanoflakes at varying potential scan rates ranging from 10 – 1000 mV/s.

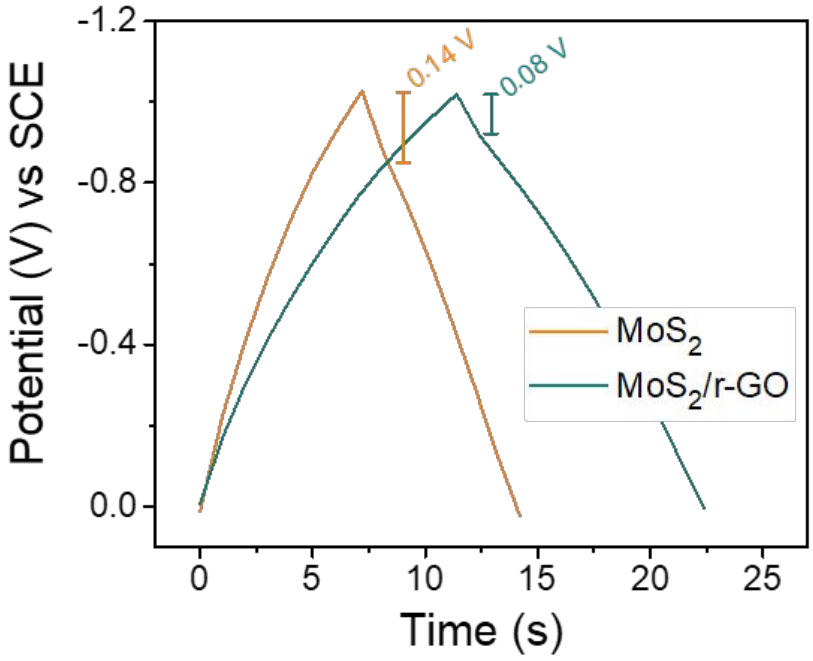

Figure S8 Comparison of galvanostatic charge-discharge (GCD) curves of the electrode materials at a current density of 5 mA/cm^2 showing bettered capacitive performance and electronic conductivity of MoS_2/r-GO electrode.

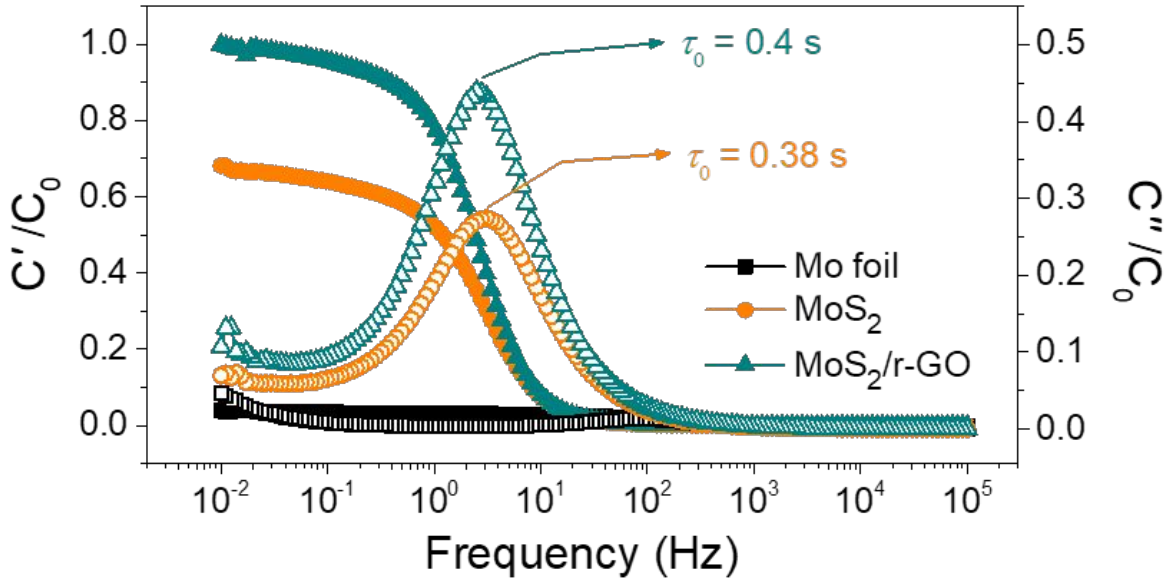

Figure S9 Plot of Real and Imaginary parts of capacitance extracted from the Nyquist plots shown in Figure 3(a).

Improvement in charge storage capacity of the hybrid material can also be validated by calculating normalized real capacitance (C'/C_0) (C_0 is the highest value among the samples).

Here, real and imaginary parts of capacitances are calculated using equations as follows:

$C' = -Z'' / (2\pi f |Z|^2)$ and $C'' = Z' / (2\pi f |Z|^2)$, where $|Z|$ is the absolute value of impedance (Ohm), Z' and Z'' are real and imaginary parts of impedance, and f is the frequency (Hz).

Although MoS_2/r-GO shows enhanced capacitive performance compared to MoS_2, both the materials behave like ideal capacitor up to frequency of 2 Hz, after that capacitance starts fading and samples behave as resistors. Further, the relaxation time constant (τ_0) which is a quantitative measure of how quickly a capacitor can be discharged is derived from the peak frequency (f_0) of the C''/C_0 *vs*. frequency plot. The relaxation time constant defines the boundary line between capacitive (at frequencies below $1/\tau_0$) and predominant resistive (at frequencies above $1/\tau_0$) behavior with varying frequencies.

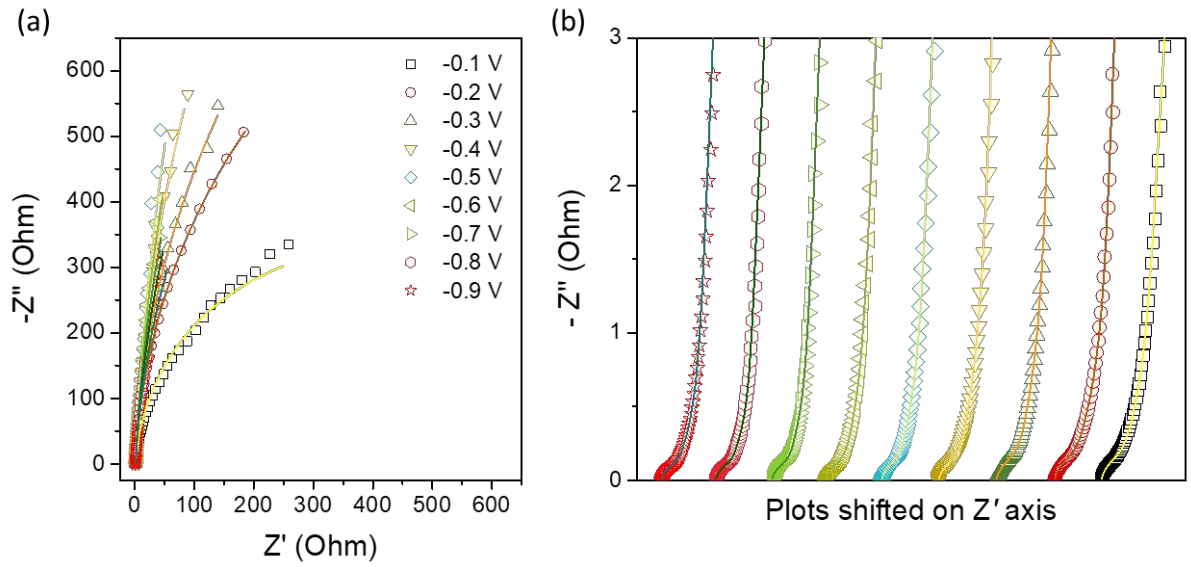

Figure S10 (a) Nyquist plots of MoS_2/r-GO hybrid at different applied potentials (scattered points) and the fitted curves (solid lines) using circuit model shown in Figure 3(b); (b) high-frequency region of Nyquist plots shown in (a).

After calculating T_{CPE} and n by fitting Nyquist plots with the equivalent circuit, the true capacitance can be calculated from T_{CPE} using the expression:

$C = R^{(\frac{1-n}{n})} T_{CPE}^{(\frac{1}{n})}$, where R is the resistance associated with the impedance.

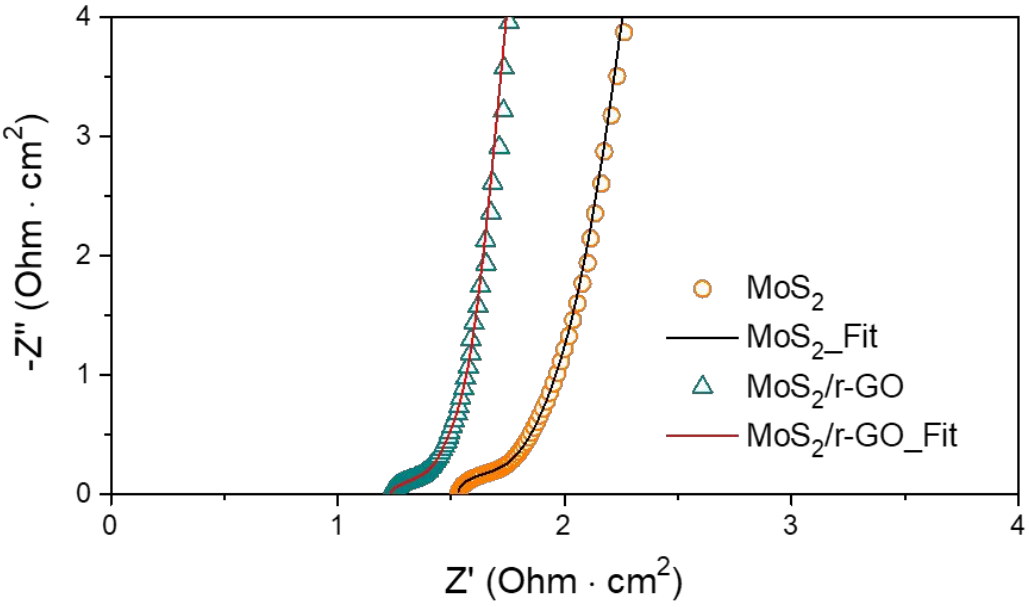

Figure S11 Fitting of Nyquist plots for MoS_2 and MoS_2/r-GO electrodes with the equivalent circuit model shown in Figure 3(b).

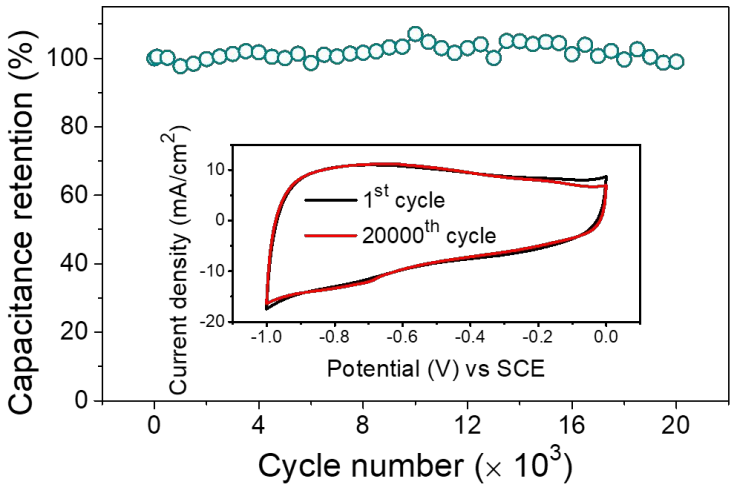

Figure S12 Cycling performance of MoS_2/r-GO electrode material evaluated over 20,000 CV cycles at a scan rate of 100 mV/s. Inset figure shows 1st and last CV cycles during the test.

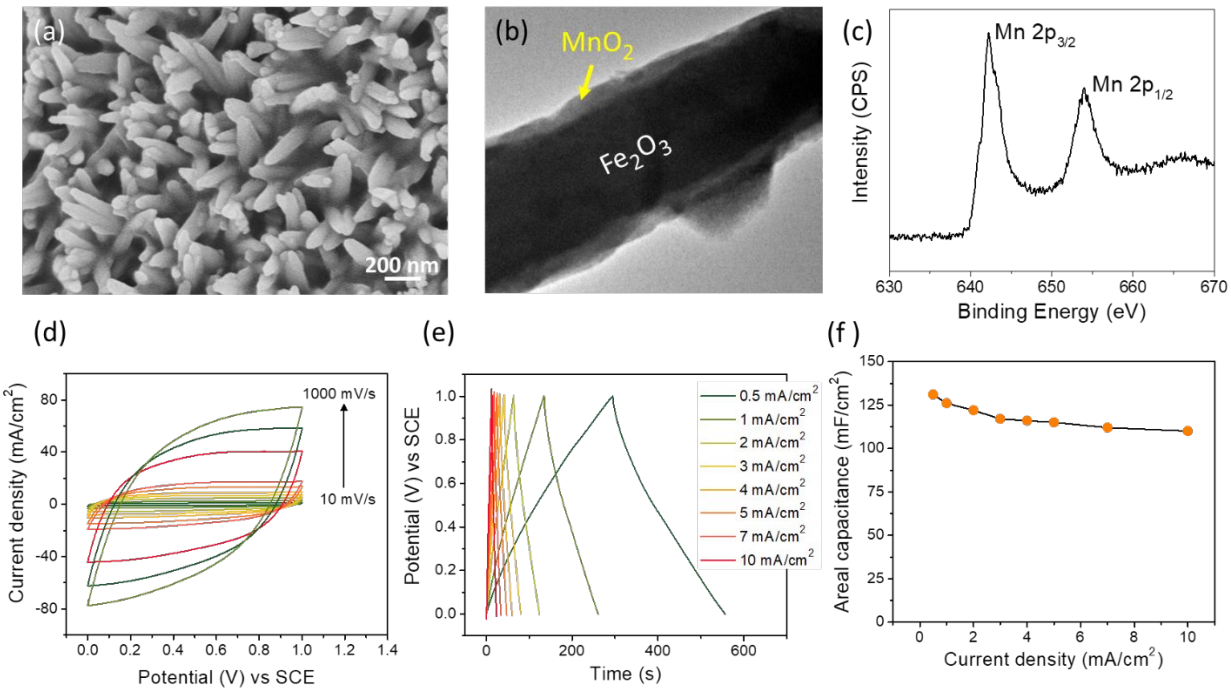

Figure S13 Morphological and structural characterization of Fe_2O_3/MnO_2 core/shell nanorods (NRs): (a) SEM image of core/shell NRs, (b) TEM image of a single NR showing the core/shell structure, (c) Mn 2p XPS spectra exhibits two prominent peaks around binding energies of 642.2 eV and 654.0 eV, which correspond to the spin-orbit doublets of Mn $2p_{3/2}$ and Mn $2p_{1/2}$, respectively, of tetravalent Mn-oxide; Electrochemical characterization of the core/shell NR electrode: (d) CV at different scan rates, (e) GCD profiles at varying current densities, and (f) variation of areal capacitance *vs*. current densities.

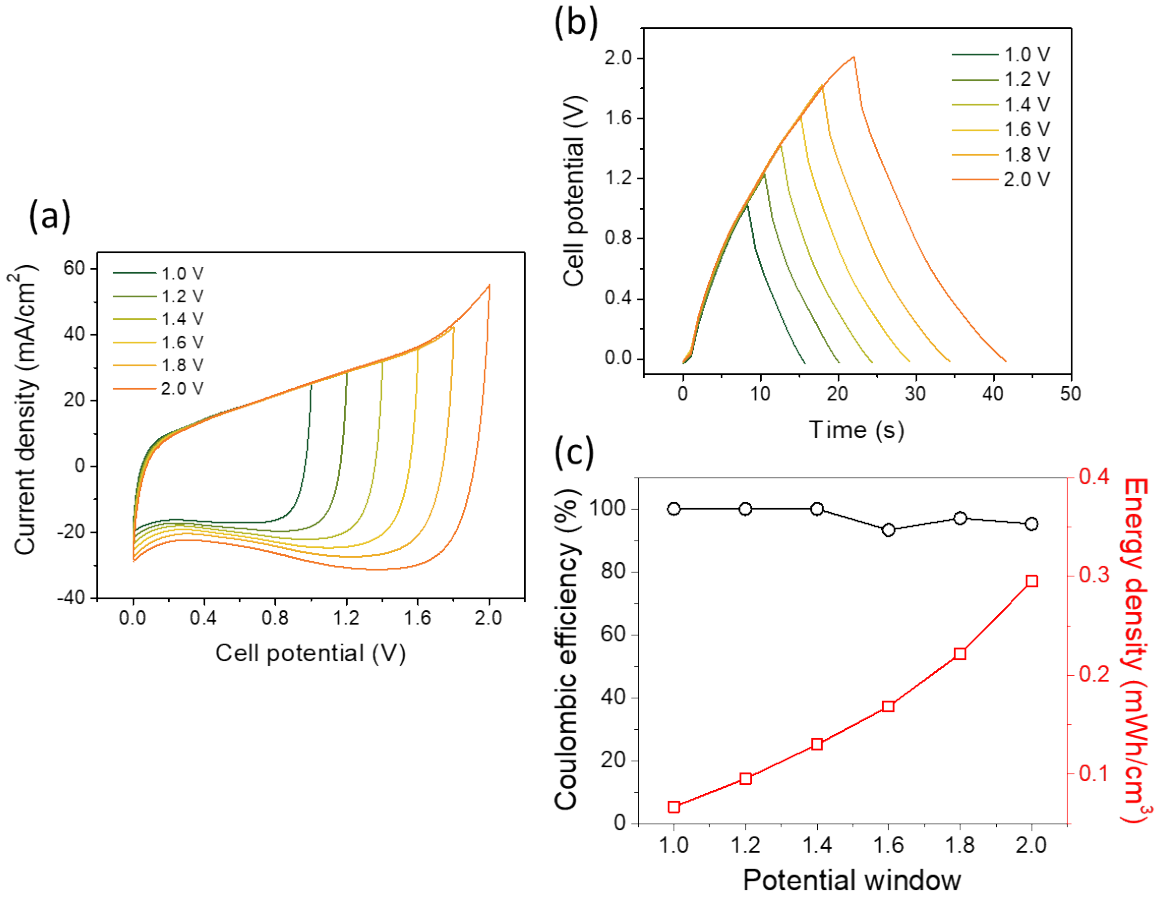

Figure S14 Tests for choosing operating potential window of MoS_2/r-GO//Fe_2O_3/MnO_2 hybrid ASC in aqueous electrolyte: (a) CV curves within different potential windows at a scan rate of 500 mV/s; (b) GCD curves at varying potential windows at a current density of 2 mA/cm^2; and (c) variation of coulombic efficiency and evolution of energy density with increasing cell potential from 1V to 2V.

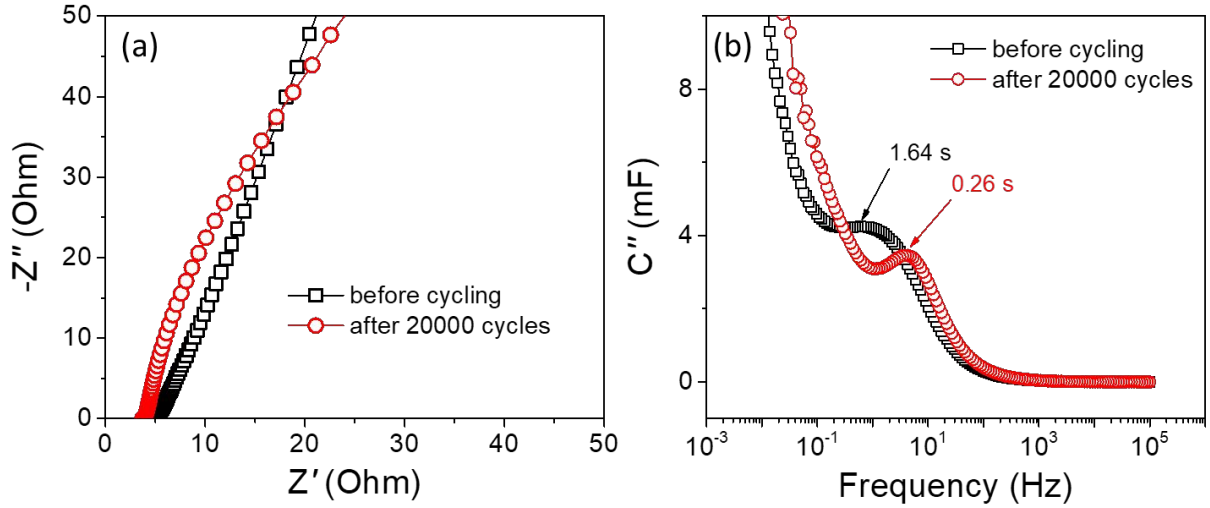

Figure S15 Impedance analyses of the ASC before and after the cycling test.